

DOE/BC/15105-4  
(OSTI ID: 780438)

INTEGRATED OUTCROP AND SUBSURFACE STUDIES OF THE  
INTERWELL ENVIRONMENT OF CARBONATE RESERVOIRS:  
CLEAR FORK (LEONARADIAN AGE) RESERVOIRS, WEST TEXAS  
AND NEW MEXICO

Semi-Annual Report  
October 1, 2000-March 31, 2001

By:  
Zeno Philip  
James W. Jennings, Jr.

Date Published: May 2001

Work Performed Under Contract No. DE-AC26-98BC15105

The University of Texas at Austin  
Austin, Texas



**National Energy Technology Laboratory  
National Petroleum Technology Office  
U.S. DEPARTMENT OF ENERGY  
Tulsa, Oklahoma**

#### **DISCLAIMER**

This report was prepared as an account of work sponsored by an agency of the United States Government. Neither the United States Government nor any agency thereof, nor any of their employees, makes any warranty, expressed or implied, or assumes any legal liability or responsibility for the accuracy, completeness, or usefulness of any information, apparatus, product, or process disclosed, or represents that its use would not infringe privately owned rights. Reference herein to any specific commercial product, process, or service by trade name, trademark, manufacturer, or otherwise does not necessarily constitute or imply its endorsement, recommendation, or favoring by the United States Government or any agency thereof. The views and opinions of authors expressed herein do not necessarily state or reflect those of the United States Government.

This report has been reproduced directly from the best available copy.

DOE/BC/15105-4  
Distribution Category UC-122

Integrated Outcrop and Subsurface Studies of the Interwell Environment of Carbonate  
Reservoirs: Clear Fork (Leonardian Age) Reservoirs, West Texas and New Mexico

By  
Zeno Philip  
James W. Jennings, Jr.

May 2001

Work Performed Under Contract DE-AC26-98BC15105

Prepared for  
U.S. Department of Energy  
Assistant Secretary for Fossil Energy

Robert E. Lemmon, Project Manager  
National Petroleum Technology Office  
P.O. Box 3628  
Tulsa, OK 74101

Prepared by  
Bureau of Economic Geology  
The University of Texas at Austin  
P.O. Box 7726  
University Station  
Austin, TX 78713

# TABLE OF CONTENTS

Abstract.....	1
Introduction.....	1
Fracture-Pattern Generation.....	2
Modeling Flow through Fractures .....	3
First Test Case: Two Staggered Fractures at the Edges of a Gridded Region: (Effect of Grid Refinement).....	8
Second Test Case: Multiple Fractures in a Staggered Array .....	9
Simulated Fracture-Pattern Cases .....	10
Summary and Conclusions .....	14
References.....	14

## **SEMI-ANNUAL TECHNICAL PROGRESS REPORT**

for

### **INTEGRATED OUTCROP AND SUBSURFACE STUDIES OF THE INTERWELL ENVIRONMENT OF CARBONATE RESERVOIRS: CLEAR FORK (LEONARADIAN AGE) RESERVOIRS, WEST TEXAS AND NEW MEXICO**

Contract No. DE-AC26-98C15105

#### **Abstract**

A major goal of this project is to evaluate the impact of fracture porosity on performance of the South Wasson Clear Fork reservoir. Our approach is to use subcritical crack (SCC) index measurements and a crack-growth simulator to model potential fracture geometries in this reservoir. We have measured the SCC index on representative rock samples and are proceeding with other pertinent rock measurements. An approach for modeling coupled matrix and fracture flow using nonneighbor connections in a traditional finite-difference simulator has been tested and found to be feasible. Accuracies within 10 % of an analytical solution for a test problem are obtained if there are four grid cells between parallel fractures. We are proceeding with estimating the effective permeabilities of different fracture patterns obtained from the crack-growth simulator.

#### **Introduction**

We have completed 30 months of this project and are in the simulation phase. A reservoir model of the matrix petrophysical properties has been constructed, and simulation studies are in progress. A goal of this project is to evaluate the effect of fracture porosity on production performance, and we have gathered fracture information from outcrop and core materials. This report summarizes our efforts to introduce fracture porosity and permeability into our reservoir model.

## Fracture-Pattern Generation

Fracturing in undeformed strata can be attributed to subcritical crack (SCC) growth, in which propagation occurs at crack-tip stress intensities,  $K_I$ , below the material's fracture toughness,  $K_{IC}$  (Atkinson and Meredith, 1987). The subcritical velocity is given by the formula

$$v = v_{max} * \left( \frac{K_I}{K_{IC}} \right)^n,$$

where  $v_{max}$  is the maximum propagation velocity at  $K_I = K_{IC}$  and  $n$  is the SCC index.

It has been observed from crack-growth simulations that the value of the SCC index affects fracture-pattern development with regard to spacing, clustering, and length distributions (Olson, 1993). The SCC index has been measured with the dual torsion beam apparatus (Williams and Evans, 1973; Pletka et al., 1979) for samples from six representative layers of the South Wasson Clear Fork reservoir (table 1).

Table 1. Mean values of the SCC index for six representative layers of the South Wasson Clear Fork reservoir.

Sample depth (ft)	Type of test	No. of tests	Mean value of SCC index
6091	Dry	7	43
	Wet	5	37
6138	Dry	11	40
	Wet	3	34
6367	Dry	6	60
	Wet	12	53
6385	Dry	6	81
	Wet	3	70
6484	Dry	5	43
	Wet	1	37
6520	Dry	8	38
	Wet	10	30

Young's modulus and fracture toughness of rocks from these layers will also be measured and used as input for conducting fracture-growth simulations using a fracture-mechanics-based crack-growth simulator (Olson, 1993). The resulting fracture patterns will be gridded and flow simulations conducted to obtain an effective permeability multiplier for each layer.

### Modeling Flow through Fractures

Flow through fractures can be modeled using nonneighbor connections in a traditional finite-difference simulator (Hearn et al, 1997). The fracture patterns are gridded such that the fractures lie at the boundary between grid cells.

The matrix flow transmissibility between any two grid cells is

$$T_{x(mat)} = \frac{k_x A_x}{\Delta x},$$

where  $A_x$  is the area perpendicular to flow in the  $x$  direction, i.e.,  $\Delta y \Delta z$ , and  $k_x$  is the permeability in the  $x$  direction (fig. 1).

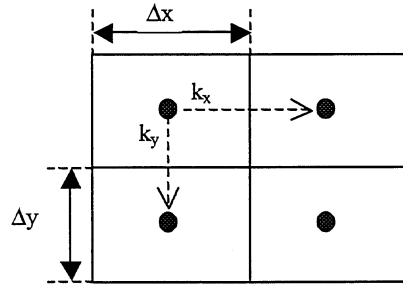


Figure 1. Schematic of grid cells indicating dimensions and permeabilities.

If there is a fracture embedded between the cells as shown in figure 2, an additional transmissibility for fracture flow can be assigned:

$$T_{x(frac)} = \frac{k_y A_y}{2 \left( \frac{\Delta y}{2} \right)} = \frac{k_y A_y}{\Delta y},$$

where  $A_y$  is the area perpendicular to flow in the  $y$  direction, i.e.,  $\Delta x \Delta z$ , and  $k_y$  is the permeability in the  $y$  direction.

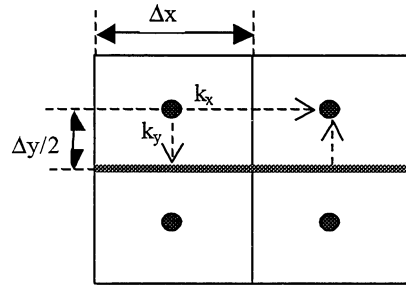


Figure 2. Schematic of grid depicting the location of a fracture.

The total x direction transmissibility, accounting for both matrix and fracture flow is

$$T_{x(total)} = T_{x(mat)} + T_{x(frac)}$$

$$= \frac{k_x A_x}{\Delta x} + \frac{k_y A_y}{\Delta y}$$

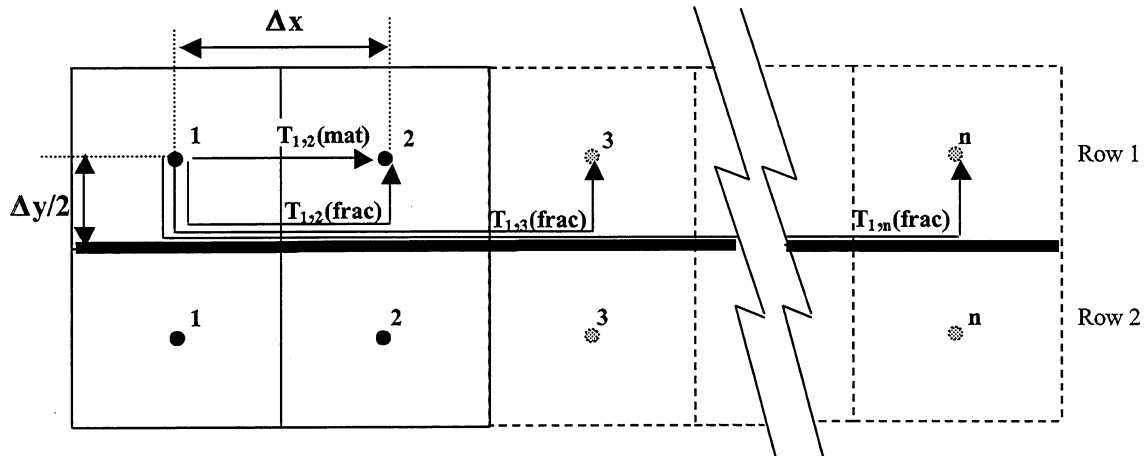


Figure 3. Array of grid cells depicting nonneighbor connections to model flow in a fracture.

The transmissibility between adjacent cells due to matrix flow is computed automatically by the simulator. Thus, for a given row, cell  $i$  is connected to cell  $i-1$  and cell  $i+1$ . The transmissibility between cells due to fracture flow can be entered explicitly using nonneighbor connections. Thus, cell  $i$  could be connected to cells  $i-1$  and  $i+1$ , as well as to all other cells on that same fracture, using an appropriate transmissibility. The

connection between cell  $i$  and its neighbors  $i-1$  and  $i+1$  is in addition to that existing because of normal matrix flow.

Thus, if there is a fracture extending between cells 1 and  $n$ , then cell 1 is connected to cells 2 through  $n$ , cell 2 is connected to cells 3 through  $n$ , and so on. The total number of nonneighbor connections per fracture is

$$\left(\frac{n(n-1)}{2}\right)2 = n(n-1).$$

The multiplication by 2 accounts for cells on both sides of the fracture. Because the nonneighbor list can become quite large, a Fortran program has been written to create it from the endpoint locations of fractures in a fracture-pattern simulation.

Thus, for a fracture between rows 1 and 2 and extending from cells 1 to  $n$ , the  $x$  direction transmissibilities for cell connections in row 1 are

(1) between cell 1 and the others

(a) for matrix flow

$$T_{1,2}(matrix) = \frac{k_x(\Delta y \Delta z)}{\Delta x} \qquad T_{1,3}, T_{1,4}, \dots, T_{1,n}(matrix) = 0$$

(b) for fracture flow

$$T_{1,2}, T_{1,3}, \dots, T_{1,n}(fracture) = \frac{k_y(\Delta x \Delta x)}{\Delta y}$$

(2) between cell 2 and the others

(a) for matrix flow

$$T_{2,3}(matrix) = \frac{k_x(\Delta y \Delta x)}{\Delta x} \qquad T_{2,4}, T_{2,5}, \dots, T_{2,n}(matrix) = 0$$

(b) for fracture flow

$$T_{2,3}, T_{2,4}, \dots, T_{2,n}(fracture) = \frac{k_y(\Delta x \Delta x)}{\Delta y}$$

The transmissibilities for cell connections in row 2 are computed similarly.

In order to verify the validity of this method, 2-D, single-phase, flow simulations were compared with an analytical solution for effective permeability in a staggered periodic array of fractures (Chirlin, 1985; Nakashima et al., 2000).

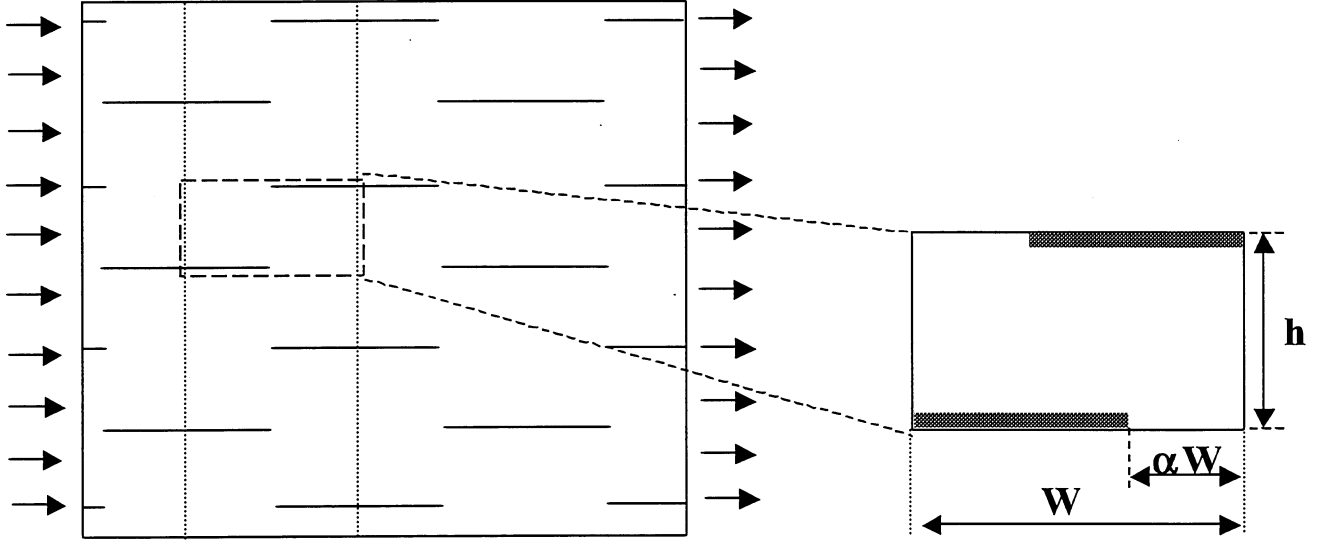


Figure 4. Chirlin's solution for a staggered array of fractures.

The effective permeability ratio  $k_{rk}$  is given by

$$k_{rk} = \frac{k_{eff}}{k} = \frac{2WK(r)}{hK(\sqrt{1-r^2})}$$

where  $K$  is the complete elliptic integral of the first kind and  $r$  is the modulus of the elliptic integral given by

$$\frac{1}{r} = \frac{2m(P-1)^2}{(mP+1)^2} + 1 + \sqrt{\left[ \frac{2m(P-1)^2}{(mP+1)^2} + 1 \right]^2 - 1}$$

with

$$\frac{1}{P} = dn \left[ \alpha K(\sqrt{1-m^2}) \sqrt{1-m^2} \right]$$

where  $dn$  is a Jacobian elliptic function and  $m$  is the modulus of elliptic integral, obtained by solving

$$\frac{K(\sqrt{1-m^2})}{K(m)} = \frac{2W}{h}$$

The equations have been implemented in Mathematica, and the solution is plotted in figure 5.

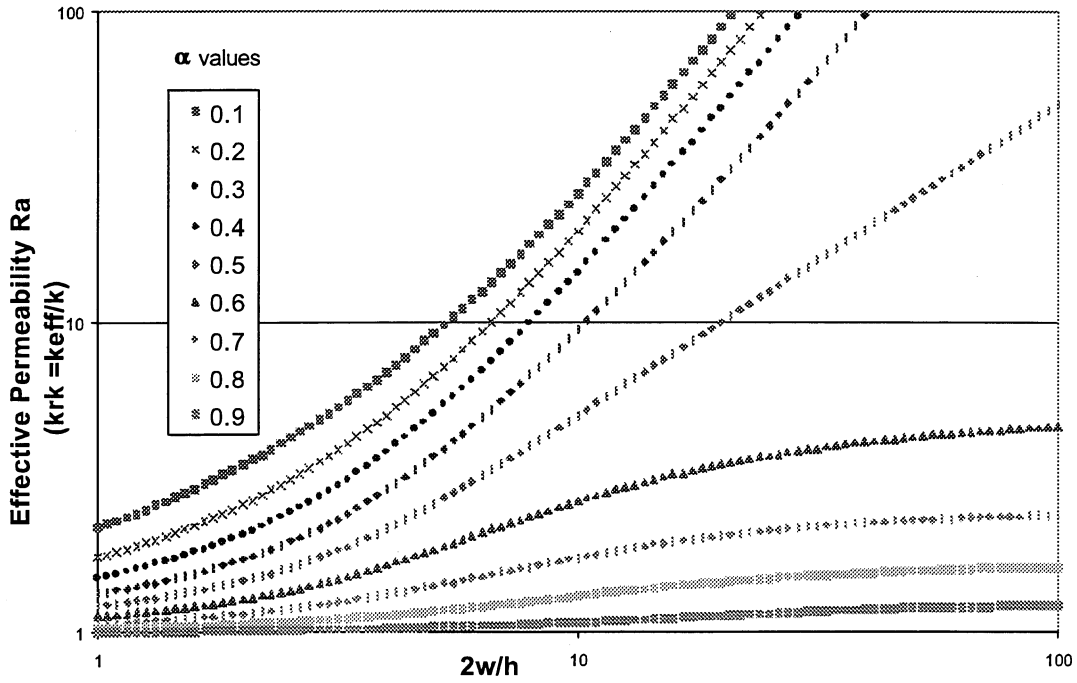


Figure 5. Chirlin's solution for effective permeability ratio for flow parallel to fractures.

Flow simulations were run until steady-state flow conditions were achieved. The effective permeability was computed from the steady-state flow rate and Darcy's law,

$$k_{eff} = \frac{q\mu L_{eff}}{A\Delta P},$$

where  $q$  is the steady-state flow rate;  $\mu$  is the fluid viscosity;  $\Delta P$  is the steady-state pressure drop across the system;  $A$  is the area perpendicular to flow, i.e.,  $\Delta x^*(\Delta y^* \text{ no. of } y \text{ cells})$ ; and  $L_{eff}$  is the length of the model minus the  $x$  dimension of one grid cell, i.e.,  $L - \Delta x$

Values of  $k_{rk} = \frac{k_{eff}}{k_{matrix}}$  obtained in this manner are compared with those obtained

from the analytical solution.

**First Test Case: Two Staggered Fractures at the Edges of a Gridded Region:  
(Effect of Grid Refinement)**

For the first test case, we used a width,  $W$ , of 4.5 ft, a fracture spacing,  $h$ , of 4.5 ft, and a fracture length of 3 ft  $[=(1-\alpha)*W]$ . This gives an  $\alpha$  value of  $\frac{1}{3}$  (fig. 6). For

$\alpha = \frac{1}{3}$  and  $\frac{2W}{h} = 2.0$  the analytical solution is  $k_{rk} = 1.947$ . The simulation results are as follows:

- (a)  $9 \times 9$  grid:  $\Delta x, \Delta y = 0.5$  ft;  $k_{rk} = 1.732$
- (b)  $18 \times 18$  grid:  $\Delta x, \Delta y = 0.25$  ft;  $k_{rk} = 1.872$
- (c)  $36 \times 36$  grid:  $\Delta x, \Delta y = 0.125$  ft;  $k_{rk} = 1.927$

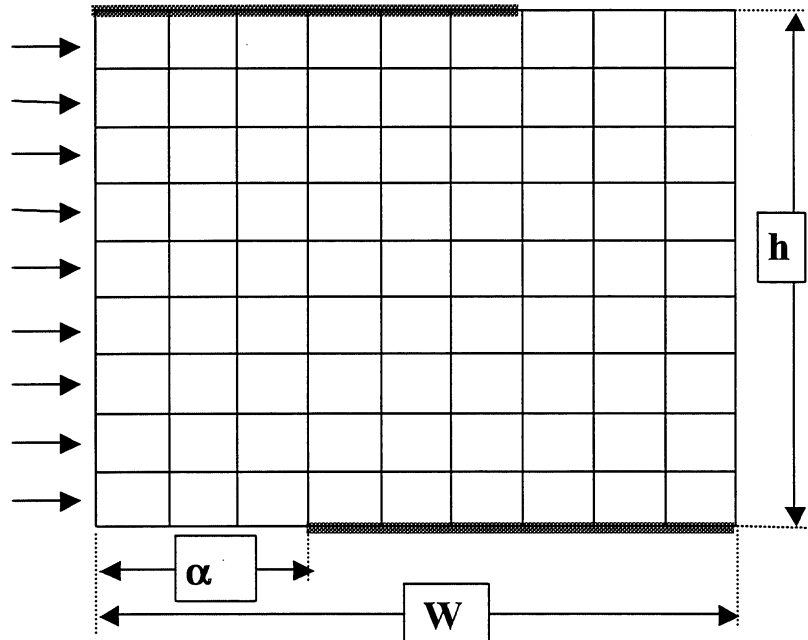


Figure 6. Gridded  $9 \times 9$  array with two edge fractures.

As the grid becomes finer in resolution, the effective permeability obtained by the flow simulation approaches the analytical solution.

### Second Test Case: Multiple Fractures in a Staggered Array

For the second test case we had multiple fractures inside the gridded region. The dimensions were the same as for the previous case, with a width,  $W$ , of 4.5 ft and an  $\alpha W$  of 1.5 ft, which implied that  $\alpha = \frac{1}{3}$ . The fracture spacing,  $h$ , however, varied according to the number of fractures. We modeled this case using three gridding schemes,  $9 \times 9$ ,  $18 \times 18$  and  $36 \times 36$ . (fig. 7)

The simulations reveal that with approximately four grid cells between fractures it is possible to obtain an accuracy within 10 % of the analytical solution.

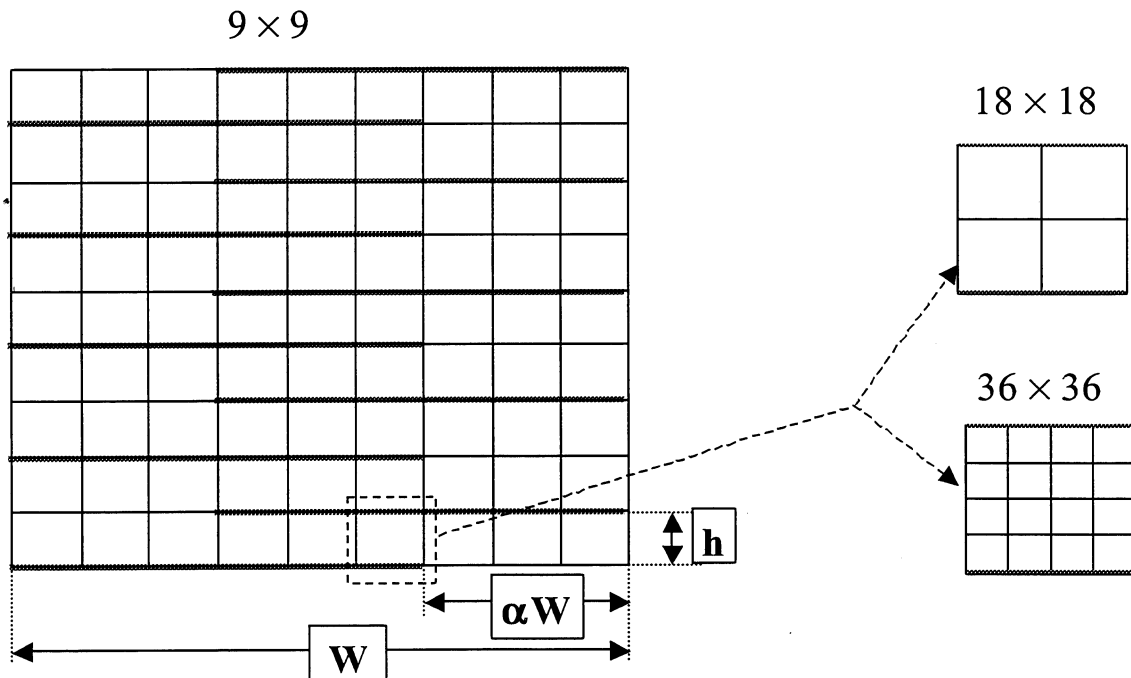


Figure 7. Gridded array with multiple fractures.

Table 2. Values of  $k_{rk}$  values and comparison between analytical solution and simulation results.

No. of fractures	$h$	$2W/h$	$k_{rk}$ values			
			Anal.so ln.	Simulation results: various grid sizes		
				$9 \times 9$	$18 \times 18$	$36 \times 36$
4	1.5	6.0	5.84	4.195	5.084	5.518
5	1.0	9.0	10.78	6.654	8.353	9.231
10	0.5	18.0	34.944	20.262	27.489	31.419

### Simulated Fracture-Pattern Cases

Sample crack-growth simulations were run for two test cases. All parameters for the crack-growth simulations were identical except for the SCC index. For case 1 it was 5 and for case 2 it was 40. The other parameters that were required as input to the crack-growth simulator were Young's modulus,  $E = 20000$  Mpa, fracture toughness,  $K_{IC} = 1.5$  MPa  $m^{1/2}$ , fracture initiation threshold,  $K_I^0 = 0.15$  MPa  $m^{1/2}$ , number of initial flaws in the modeled area = 50, strain rate =  $8.33E-19$ , and total time of loading = 3.17 million years. The resulting fracture patterns are shown in figures 8 and 9. It is evident that the higher SCC index leads to a more "clustered" fracture pattern.

Fracture end points from the simulated crack patterns were used to create the list of nonneighbor connections. Flaws that did not grow were removed from the flow simulation. With a  $60 \times 120$  gridding scheme, the number of nonneighbor connections for cases 1 and 2 were 18848 and 8322, respectively. Single-phase 2-D flow simulations were carried out with constant pressure boundary conditions and flow in the  $x$  direction. For the same  $60 \times 120$  gridding scheme, the values of  $k_{rk}$  obtained for cases 1 and 2 were 4.82 and 3.52, respectively. As expected, the more fractured pattern (case 1) was found to have a higher effective-permeability ratio.

The effect of grid refinement in the  $y$  direction was also studied. A constant  $x$  gridding size was maintained (120 for case 2 and 60 for case 1). The results are shown in

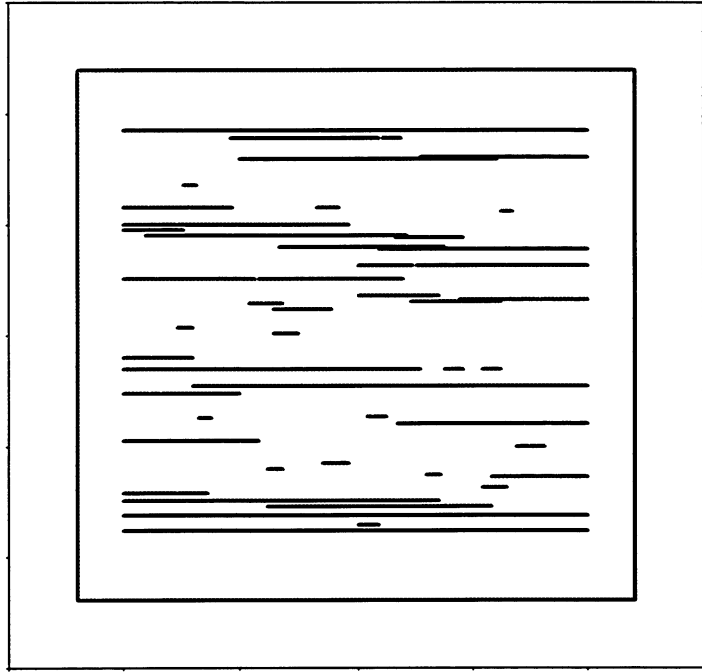


Figure 8. Case 1 simulated fracture pattern.

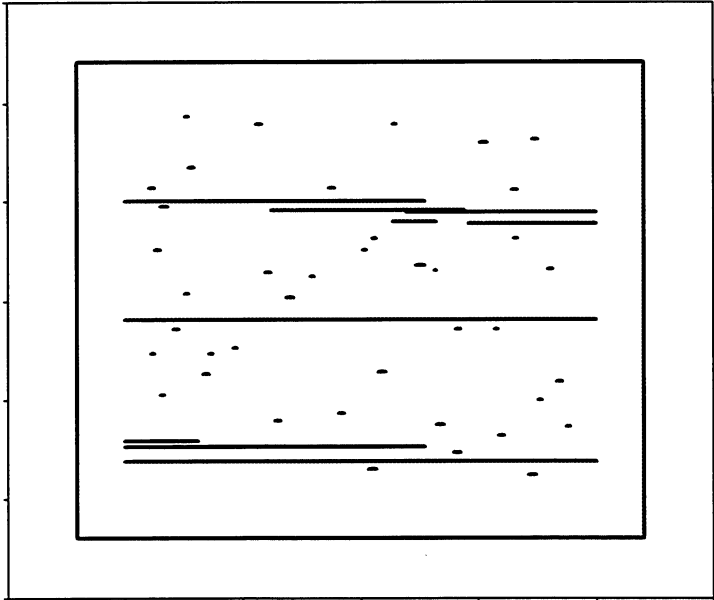


Figure 9. Case 2 simulated fracture pattern.

tables 3 and 4 ,as well as plotted in figures 10 and 11. It is evident that grid refinement does affect the effective-permeability ratio. Satisfactory results are obtained when the y gridding is 600 cells.

Table 3. Case 1. Values of  $k_{rk}$  for various gridding schemes.

Gridding scheme, 'X' × 'Y' no. of cells	Effective permeability Ratio, $k_{rk}$
60 × 60	4.984
60 × 120	4.820
60 × 240	4.743
60 × 300	4.724
60 × 600	4.680
60 × 1200	4.662
60 × 2400	4.652

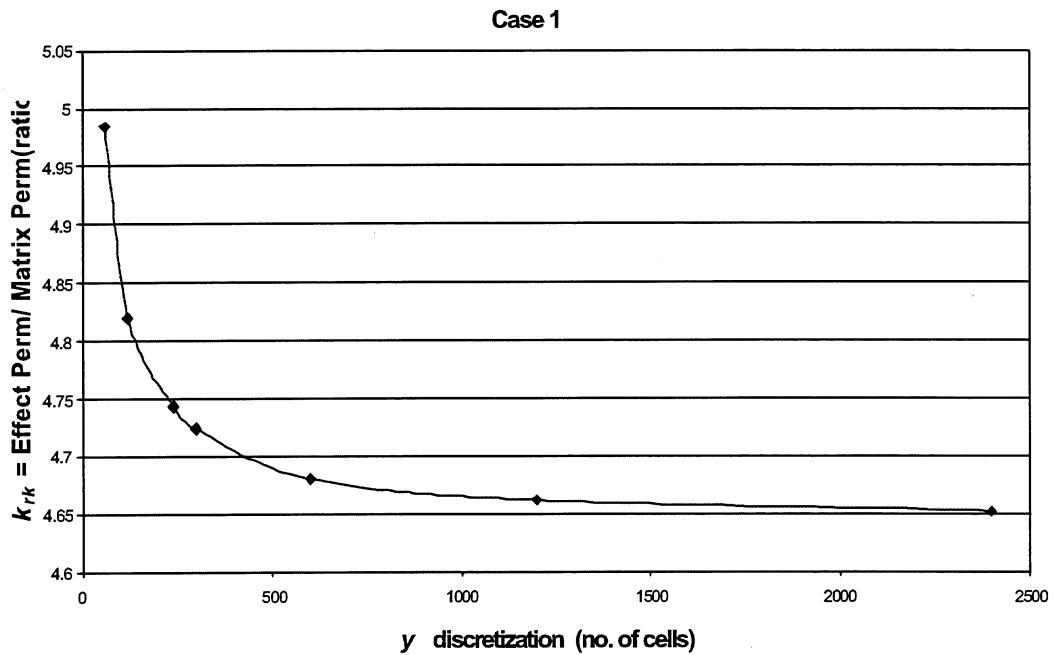


Figure 10. Case 1. Effect of y grid cell refinement on  $k_{rk}$  (constant x discretization of 60 cells).

Table 4. Case 2. Values of  $k_{rk}$  for various gridding schemes.

Gridding scheme, 'X' × 'Y' no. of cells	Effective permeability Ratio, $k_{rk}$
120 × 120	3.41
120 × 240	3.33
120 × 600	3.276
120 × 1200	3.253
120 × 2400	3.244
120 × 4800	3.239

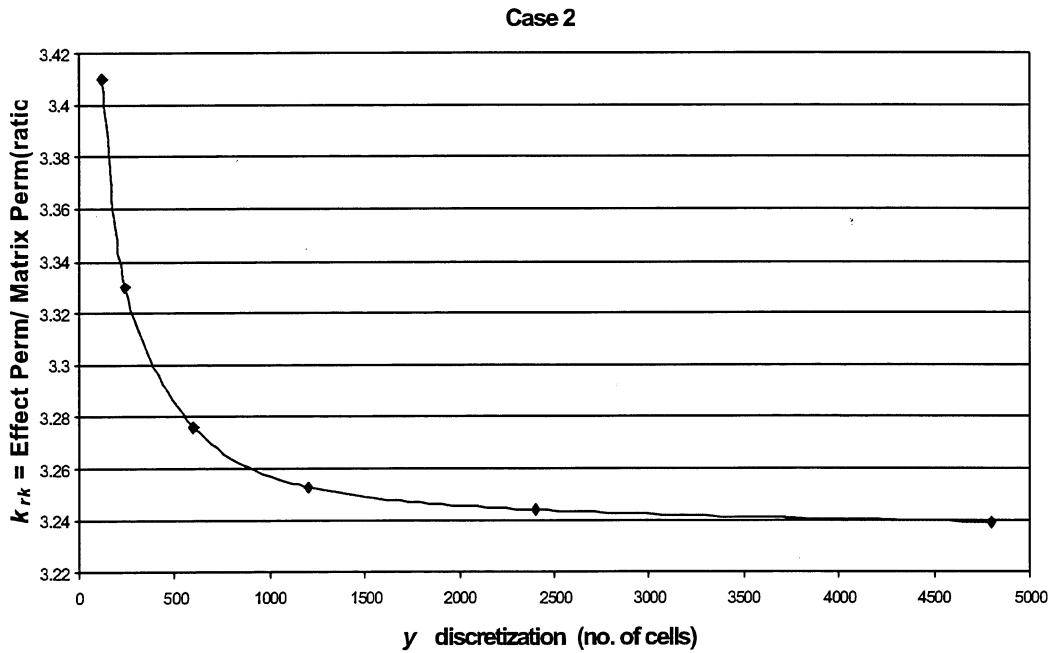


Figure 11. Case 2. Effect of  $y$  grid cell refinement on  $k_{rk}$  (constant  $x$  discretization of 120 cells).

### Summary and Conclusions:

- (1) We have measured the SCC index on representative rock samples and are proceeding with other pertinent rock measurements.
- (2) An approach for coupling matrix and fracture flow using nonneighbor connections in a traditional finite difference simulator has been tested and found to be feasible. Accuracies of within 10 % of the analytical solution are obtained if there are four grid cells between parallel fractures.
- (3) We are proceeding with estimating the effective permeabilities of different fracture patterns obtained from the crack-growth simulator.

### References

- Atkinson, B. K., and Meredith, P. G., "The theory of subcritical crack growth with applications to minerals and rocks," in *Fracture Mechanics of Rock*, edited by B. K. Atkinson, pp. 111-166, Academic, San Diego, 1987.
- Chirlin, G. R., "Flow through a Porous Medium with Periodic Barriers or Fractures," *SPEJ* (June 1985), pp. 358-362.
- Hearn, C. L., SPE, Occidental Petroleum of Qatar, Ltd., Al-Emadi, Ismail A. Abdulla, SPE, Qatar General Petroleum Corp., Worley, Paul L. H. and Taylor, R D., SPE, Occidental Petroleum of Qatar, Ltd., SPE 38908 – "Improved Oil Recovery in a Tight Reservoir with Conductive Faults, ISND Shuiaba, Qatar," presented at the 1997 SPE Annual Technical Conference and Exhibition, San-Antonio, TX, USA, 5-8 Oct., 1997.
- Nakashima, T., SPE, Waseda University, Sato, K., SPE, The University of Tokyo, Arihara, N., SPE, Waseda University, and Yazawa, N., SPE, JNOC, SPE 64286 –

“Effective Permeability Estimation for Simulation of Naturally Fractured Reservoirs,” presented at the SPE Asia Pacific Oil and Gas Conference and Exhibition held in Brisbane, Australia, 16-18 Oct., 2000.

Olson, Jon E., “Joint Pattern Development: Effects of Subcritical Crack Growth and Mechanical Crack Interaction,” *Journal of Geophysical Research*, Vol. 98, No B7, pp 12,251-12,265, 1993.

Pletka, B. J., Fuller, E. R., Jr., and Koepke, B. G., “An Evaluation of Double-Torsion Testing – Experimental,” *Fracture Mechanics Applied to Brittle Materials*. ASTM STP 678, S. W. Freiman, Ed., American Society for Testing and Materials, 1979, pp. 19-37.

Williams, D. P., and Evans, A. G., “A Simple Method for Studying Slow Crack Growth,” *Journal of Testing and Evaluation*, JTEVA, Vol. 1, No. 4, 1973, pp. 264-270.



